Electronic Supplementary Material (ESI) for Journal of Materials Chemistry A.
This journal is © The Royal Society of Chemistry 2023

Supplementary Information

Heteroatomic interface engineering of octahedron VSe_2-ZrO_2/C/MXene composite derived from MXene-MOF hybrid as superior-performance anode for lithium-ion batteries

Hanbin Li[a], Jinliang Li[b*], Liang Ma [b, c*], Xinlu Zhang[d], Junfeng Li[e], Jiabao Li[f], Ting Lu[a], Likun Pan[a*]

[a] *Shanghai Key Laboratory of Magnetic Resonance, School of Physics and Electronic Science, East China Normal University, Shanghai 200241, China*

[b] *Siyuan Laboratory, Guangzhou Key Laboratory of Vacuum Coating Technologies and New Energy Materials, Guangdong Provincial Engineering Technology Research Center of Vacuum Coating Technologies and New Materials, Department of Physics, Jinan University, Guangzhou, Guangdong 510632, China*

[c] *School of Chemistry, Guangzhou Key Laboratory of Materials for Energy Conversion and Storage, South China Normal University, Guangzhou 510006, China*

[d] *Key Laboratory for Liquid-Solid Structural Evolution & Processing of Materials (Ministry of Education), Research Center for Carbon Nanomaterials, School of Materials Science and Engineering, Shandong University, Jinan 250061, China*

[e] *College of Logistics Engineering, Shanghai Maritime University, Shanghai 201306, China*

[f] *School of Chemistry and Chemical Engineering, Yangzhou University, Yangzhou, Jiangsu 225002, China*

**Corresponding author:*

E-mail address: lkpan@phy.ecnu.edu.cn (L. Pan), lijinliang@email.jnu.edu.cn (J. Li), maliang2415@jnu.edu.cn (L. Ma).

Materials

Hydrofluoric acid (HF, 40%), zirconium tetrachloride ($ZrCl_4$, 98%), terephthalic acid (H_2BDC, 99%), N, N-Dimethylformamide (DMF, ≥99.5%), glacial acetic acid (GR, ≥99.8%) and selenium powder (Se, ≥99.0%) were supplied by Sinopharm Chemical Reagent Co. Ltd. Vanadium aluminum carbide (V_2AlC, 98%, 400 mesh) was purchased from Jilin 11 Technology Co. Ltd.

Characterizations

The morphologies and interior structure were detected by field-emission scanning electron microscopy (FESEM, Tescan Mira 3 XH) and transmission electron microscopy (TEM, JEOL-2100F). X-ray diffraction spectroscopy (XRD, D/Max-2500/PC, RIGAKU, Japan) for measuring the phase structure was conducted with Cu Kα radiation (λ = 0.15406 nm). The specific surface areas and pore size distributions were acquired by the nitrogen adsorption-desorption measurements on the AutosorbiQ analyzer (Quantachrome, USA). X-ray photoelectron spectroscopy (XPS) was collected in Escalab 250Xi spectrometer with Al Kα radiation (hν=1486.6eV). Electron paramagnetic resonance (EPR) spectra were obtained on Bruker ELEXSYS E580 spectrometer with a super high sensitivity cavity. Thermogravimetric analysis (TGA) was tested by thermal gravimetric analyzer (Mettler Toledo, Switzerland). The content of element was determined by inductively coupled plasma-atomic emission spectrometry (ICP-AES, Pe Avio200). Raman spectra were obtained using a laser of 532 nm by Raman microscope (XploRA PLUS).

Battery fabrication and electrochemical measurements

To study the electrochemical properties of half cells, the active materials, Super P and polyvinylidene fluoride (PVDF) were mixed in an agate mortar at a mass ratio of 8:1:1 into moderate N-methyl-2-pyrrolidinone (NMP) solvent to obtain the

homogeneous slurry. Then, the slurry was bladed onto Cu foil and dried at 110 ℃ for 12 h under vacuum. The dried foil was cut into a circular electrode with a diameter of 14 mm on which the mass loading of the active material was 1.2-1.4 mg. The half coin cells (CR2032) were assembled in an argon-filled glove box with both the moisture and the oxygen content below 0.5 ppm. The electrolyte was formed by $LiPF_6$ (1.0 M) in ethylene carbonate/dimethyl carbonate /ethyl methyl carbonate (1:1:1 in volume), while Li disc was applied as a counter electrode and glass membrane as a separator. Galvanostatic charge/discharge measurements were conducted in the LAND CT2001A battery testing system setting the voltage range of 0.01 V-3.0 V. Cyclic voltammetry (CV) curves were investigated in the electrochemical workstation (AUTO-LAB PGSTAT302N) with the same voltage range at a scan rate of 0.2 mV s^{-1} unless otherwise noted. Electrochemical impedance spectroscopy (EIS) data were recorded in the same electrochemical workstation with the frequency ranging from 0.01 to 100 kHz.

For full cells, the cathode was prepared in the same technique as the anode except for the active material of commercial $LiFePO_4$ and the Al foil current collector. For the testing of the full cell, the voltage window was set as 1.5-3.5 V with a designed anode/cathode reversible capacity ratio of ~1.1. Both the current density and specific capacity were calculated based on the mass of the anode.

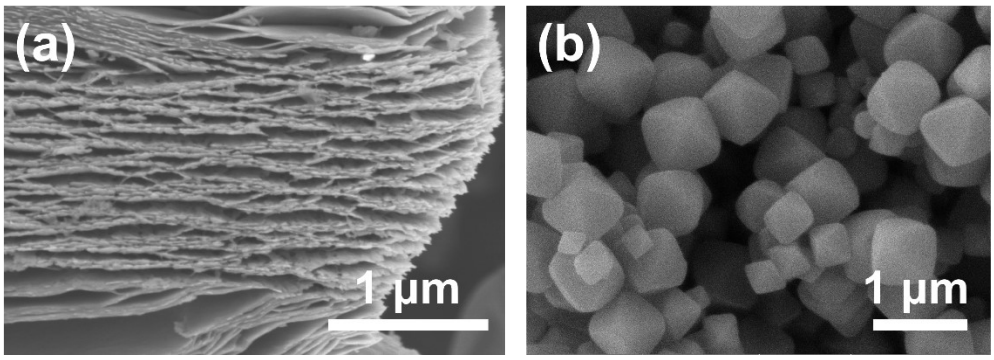

Fig. S1. FESEM images of (a) V_2CT_x and (b) UiO-66.

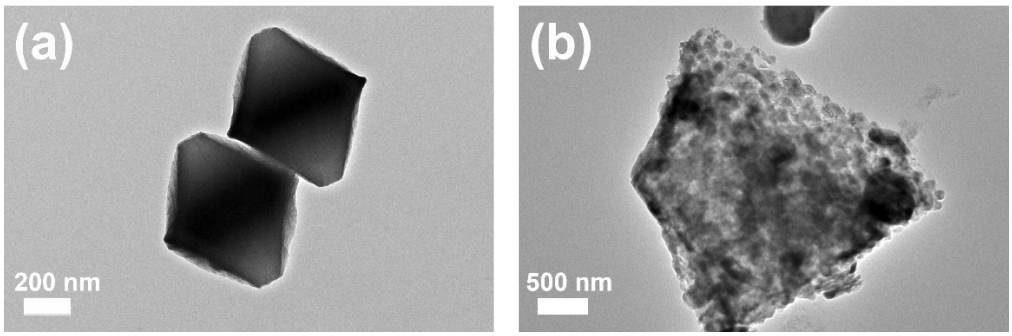

Fig. S2. TEM images of (a) Se-ZrO_2/C and (b) VSe_2/MXene.

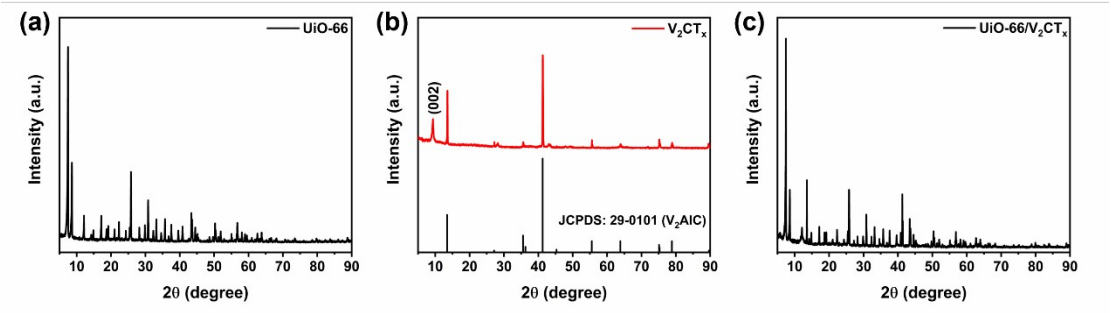

Fig. S3. XRD patterns of (a) UiO-66, (b) V_2CT_x and (c) UiO-66/V_2CT_x.

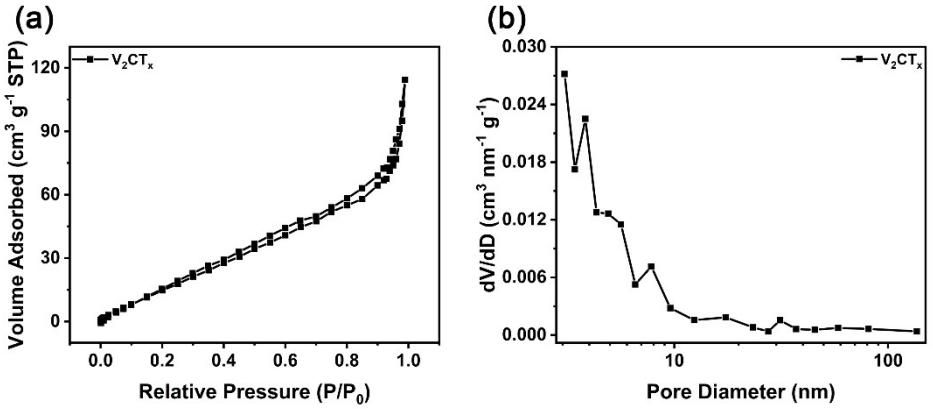

Fig. S4. (a) Nitrogen adsorption-desorption isotherms and (b) pore size distributions of V_2CT_x.

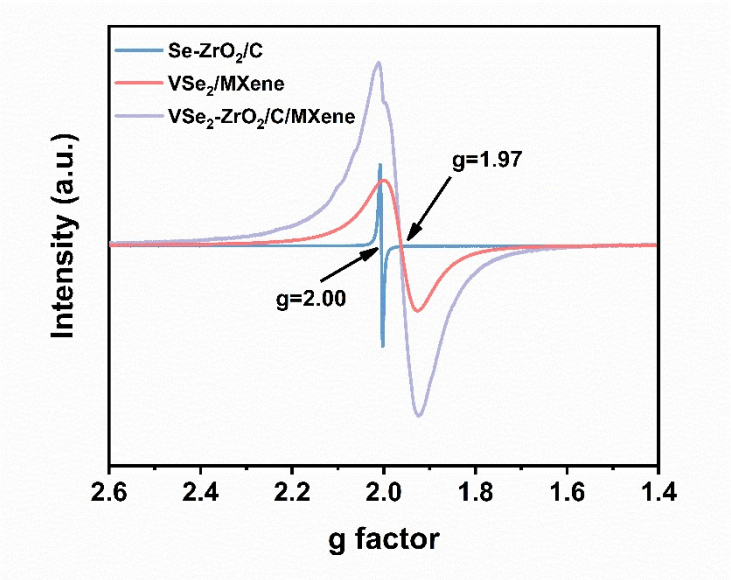

Fig. S5. EPR spectra of Se-ZrO_2/C, VSe_2/MXene and VSe_2-ZrO_2/C/MXene.

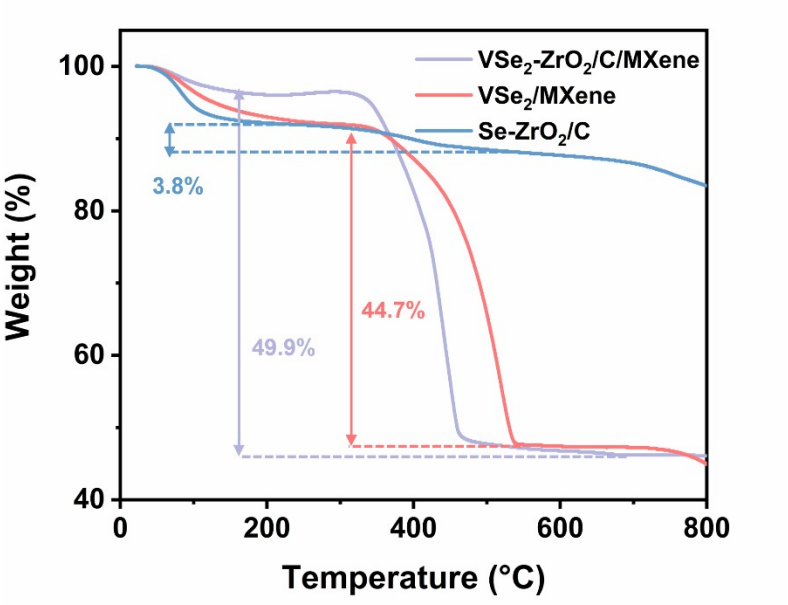

Fig. S6. TGA curves of Se-ZrO_2/C, VSe_2/MXene and VSe_2-ZrO_2/C/MXene.

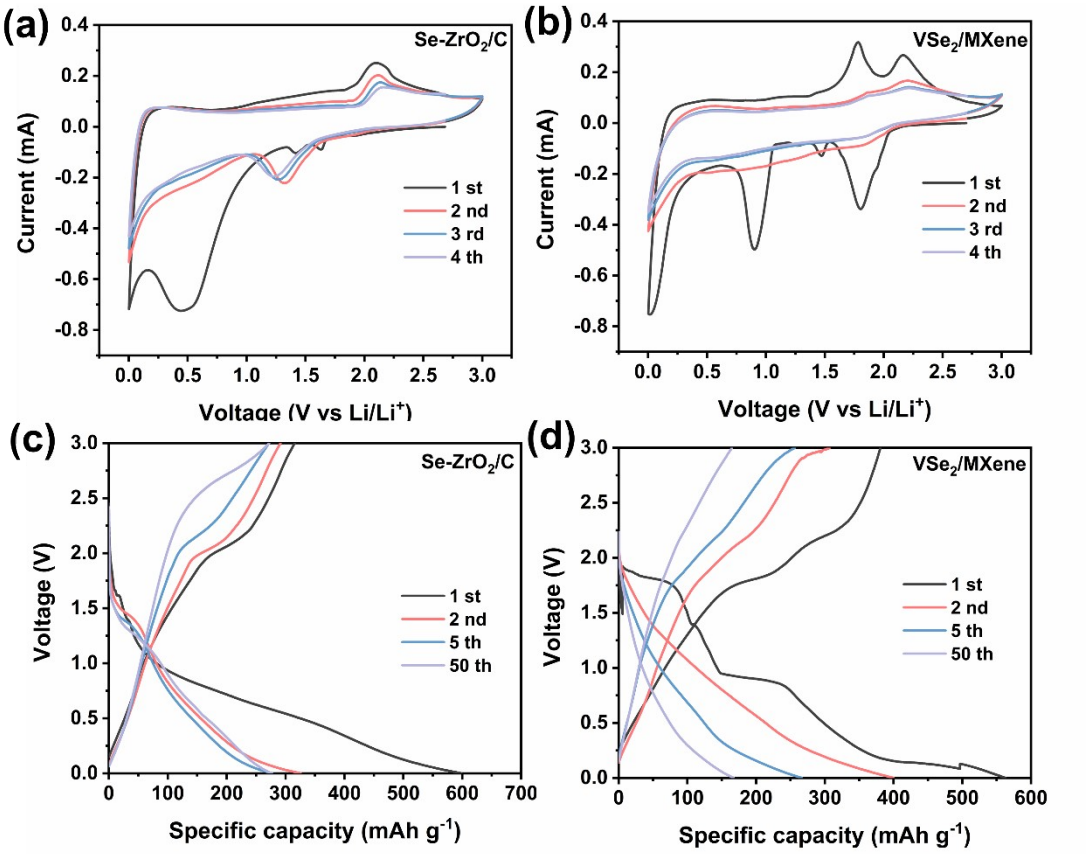

Fig. S7. CV curves at 0.2 mV s^{-1} of (a) Se-ZrO_2/C and (b) VSe_2/MXene. GCD profiles of (c) Se-ZrO_2/C and (d) VSe_2/MXene.

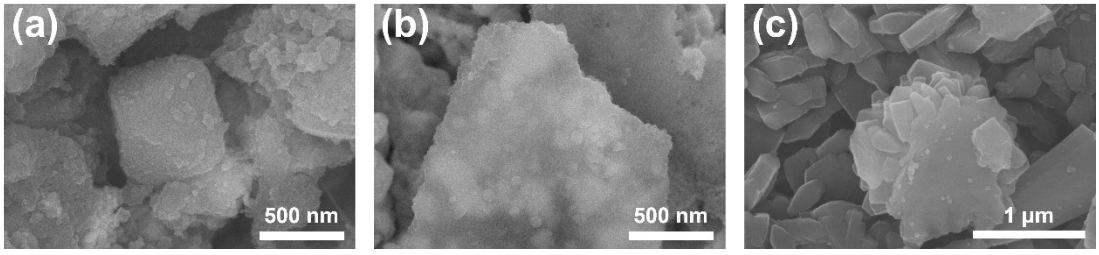

Fig. S8. FESEM images of VSe_2-ZrO_2/C/MXene, VSe_2/MXene and Se-ZrO_2/C electrodes after 100 cycles at the current density of 100 mA g^{-1}.

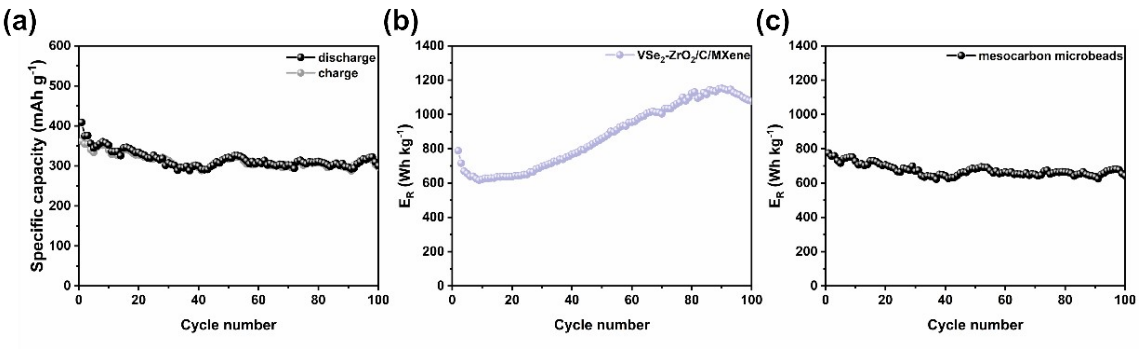

Fig. S9. (a) Cycling performance of meso-carbon microbeads. (b) and (c) Charge E_R of VSe_2-ZrO_2/C/MXene and meso-carbon microbeads.

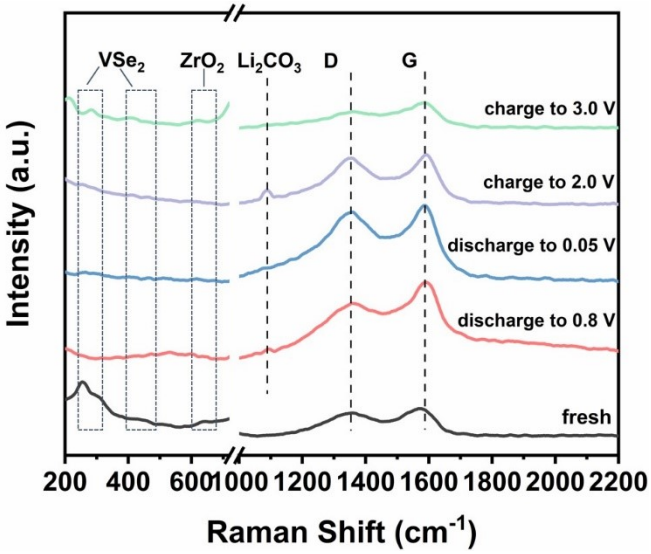

Fig. S10. Ex-situ Raman spectra of VSe_2-ZrO_2/C/MXene anode at different potential states.

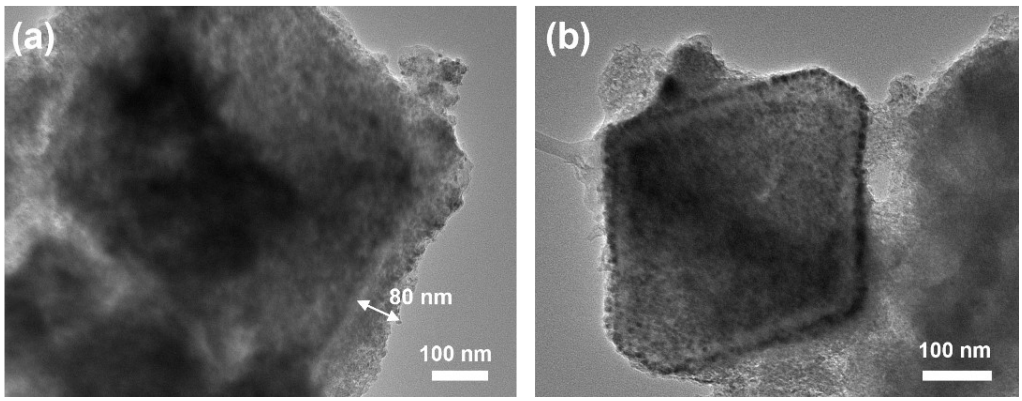

Fig. S11. TEM images of VSe_2-ZrO_2/C/MXene electrode after (a) discharging to 0.05 V and (b) charging to 3.0 V.

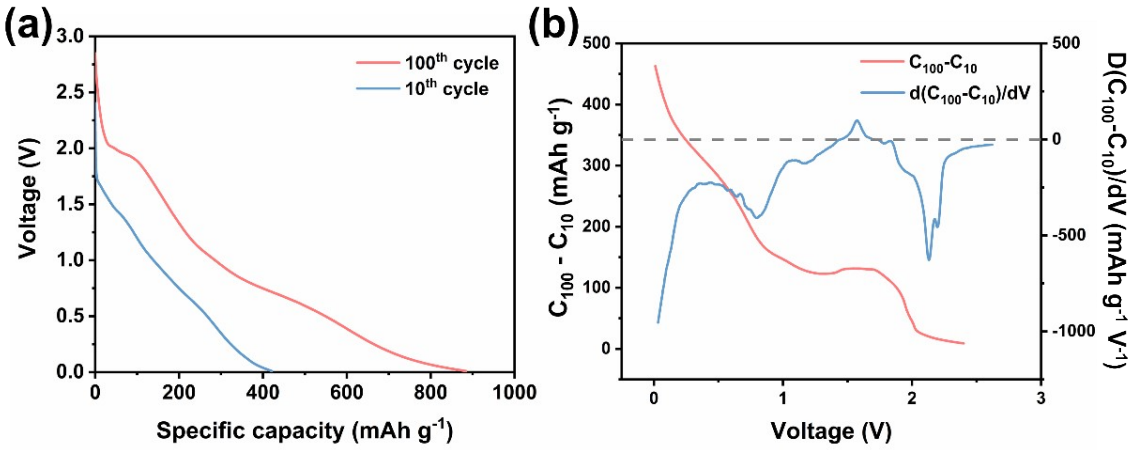

Fig. S12. (a) Discharge profiles for VSe_2-ZrO_2/C/MXene at the 10th and 100th cycles. (b) Difference of the capacities at the 10th and 100th cycles and their differential vs. voltage.

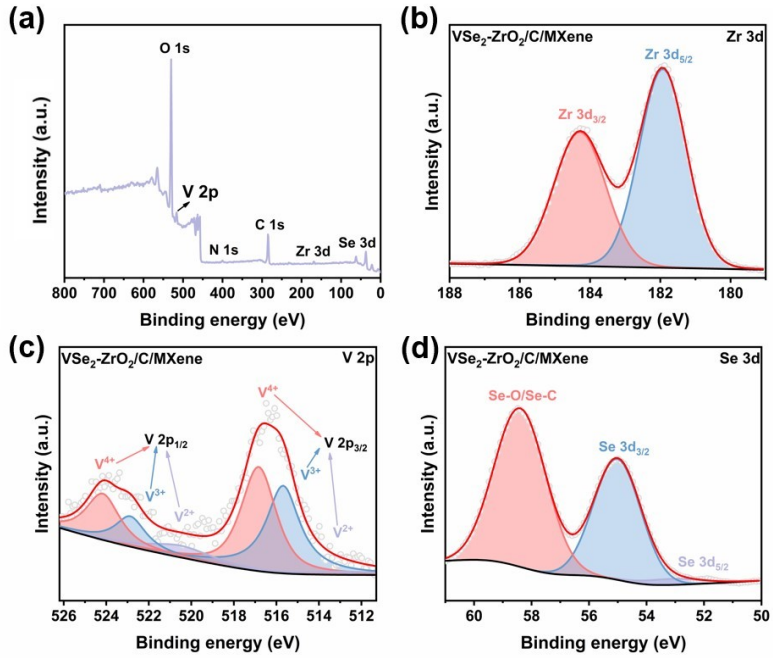

Fig. S13. (a) Survey, (b) Zr 3d, (c) V 2p and (d) Se 3d XPS spectra for VSe_2-ZrO_2/C/MXene after cycling.

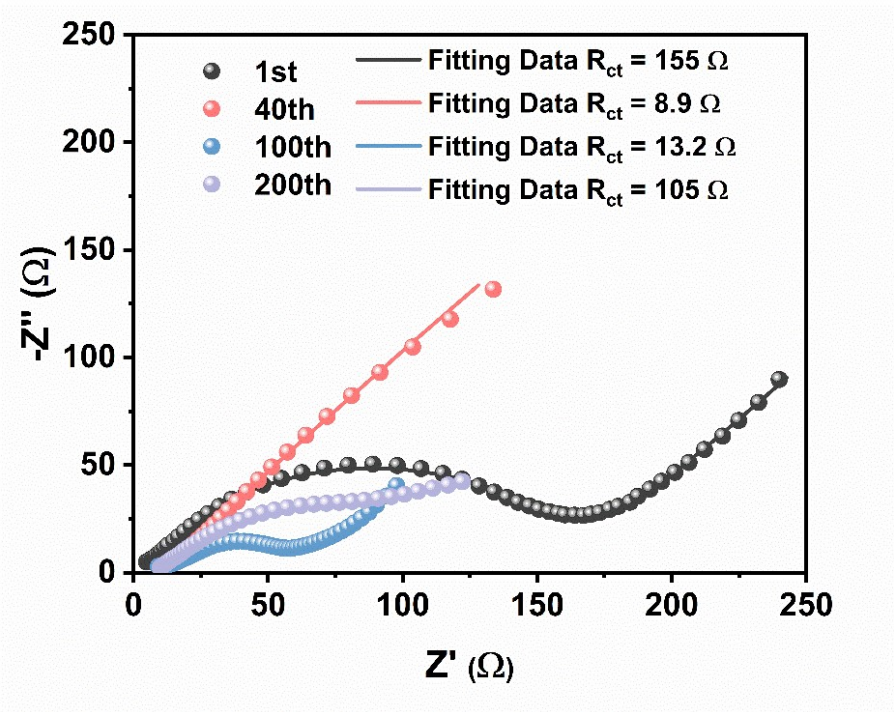

Fig. S14. Nyquist plots of VSe_2-ZrO_2/C/MXene after different cycles.

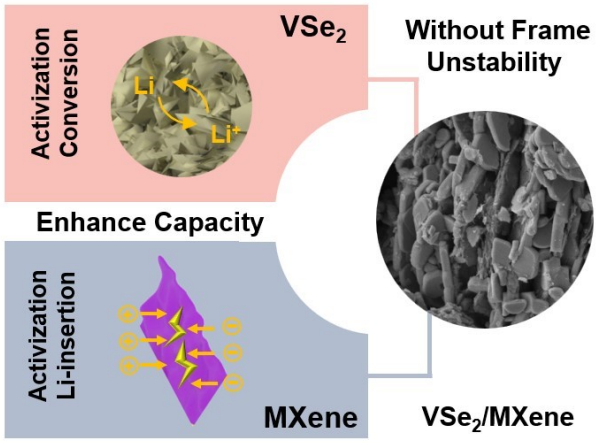

Fig. S15. Schematic of VSe_2/MXene for Li-ion storage mechanism.

Table S1 Atomic concentration (at. %) of elements detected from XPS measurement for Se-ZrO_2/C, VSe_2/MXene and VSe_2-ZrO_2/C/MXene.

Sample	C	N	O	Se	Zr	V
Se-ZrO_2/C	46.59	6.28	23.96	11.67	11.49	-
VSe_2/MXene	36.77	-	31.42	17.68	-	14.13
VSe_2-ZrO_2/C/MXene	52.88	3.55	17.11	12.04	6.25	8.18

Table S2 Comparison of the lithium-ion storage performances between VSe_2-ZrO_2/C/MXene in this work and similar anode materials reported in the literatures.

Sample	Current density (mA g^{-1})	Cycle number	Capacity (mAh g^{-1})	Capacity retention	refs
UiO-66	38.8	100	118	65%	[S1]
SnO_x@UiO-66	50	100	994	85%	[S2]
VSe_2-NSs	2000	70	430	-	[S3]
	100	100	1020	119%	
VSe_2 NSA/C	100	50	768	98%	[S4]
VSe_2/C	100	50	453	-	[S5]
VSe_2/graphene	100	60	630	~100%	[S6]
VSe_2-ZrO_2/C/MXene	100	210	1238.5	143%	This work

References

S1. B. Tang, S. Huang, Y. Fang, J. Hu, C. Malonzo, D. G. Truhlar and A. Stein, *J. Chem. Phys.*, 2016, **144**, 194702.

S2. W. Li, Z. Li, F. Yang, X. Fang and B. Tang, *ACS Appl. Mater. Inter.*, 2017, **9**, 35030-35039.

S3. Q. Jiang, J. Wang, Y. Jiang, L. Li, X. Cao and M. Cao, *Nanoscale*, 2020, **12**, 8858-8866.

S4. F. Ming, H. Liang, Y. Lei, W. Zhang and H. N. Alshareef, *Nano Energy*, 2018, **53**, 11-16.

S5. X. Yang and Z. Zhang, *Mater. Lett.*, 2017, **189**, 152-155.

S6. Y. Wang, B. Qian, H. Li, L. Liu, L. Chen and H. Jiang, *Mater. Lett.*, 2015, **141**, 35-38.